JCTC Journal of Chemical Theory and Computation

Article

pubs.acs.org/JCTC

Ion Binding to Quadruplex DNA Stems. Comparison of MM and QM Descriptions Reveals Sizable Polarization Effects Not Included in Contemporary Simulations

Konstantinos Gkionis,[†] Holger Kruse,[†] James A. Platts,[‡] Arnošt Mládek,[§] Jaroslav Koča,[†] and Jiří Šponer*[,†,§]

[†]CEITEC - Central European Institute of Technology, Masaryk University, Campus Bohunice, Kamenice 5, 625 00 Brno, Czech Republic

[‡]School of Chemistry, Cardiff University, Park Place, Cardiff CF10 3AT, United Kingdom

[§]Institute of Biophysics, Academy of Sciences of the Czech Republic, Královopolská 135, 612 65 Brno, Czech Republic

Supporting Information

ABSTRACT: Molecular mechanical (MM) force fields are commonly employed for biomolecular simulations. Despite their success, the nonpolarizable nature of contemporary additive force fields limits their performance, especially in long simulations and when strong polarization effects are present. Guanine quadruplex D(R)NA molecules have been successfully studied by MM simulations in the past. However, the G-stems are stabilized by a chain of monovalent cations that create sizable polarization effects. Indeed, simulation studies revealed several problems that have been tentatively attributed to the lack of polarization. Here, we provide a detailed comparison between quantum chemical (QM) DFT-D3 and MM potential energy surfaces of ion binding to G-stems and assess differences that may affect MM simulations. We suggest that MM describes binding of a single ion to the G-stem rather well. However, polarization effects become very significant when a second ion is present. We suggest that the MM approximation substantially limits accuracy of description of energy and dynamics of multiple ions inside the G-stems and binding of ions at the stem−loop junctions. The difference between QM and MM descriptions is also explored using symmetry-adapted perturbation theory and quantum theory of atoms in molecules analyses, which reveal a delicate balance of electrostatic and induction effects.

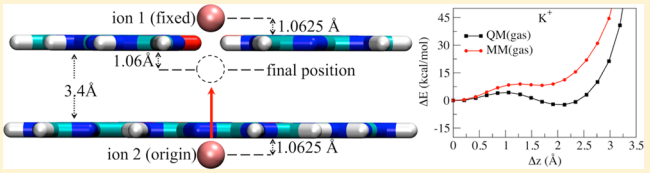

INTRODUCTION

Among the rich conformational variants of DNA, particularly interesting are guanine quadruplex structures (G-DNA) that may occur in guanine-rich DNA regions. G-DNA structures include units of planar guanine quartets with each guanine acting both as H-bond donor and acceptor with its neighboring counterparts. Consecutive stacked quartets form the G-DNA stems, which may consist of parallel or antiparallel DNA strands. G-DNA is stabilized by monovalent ions. Assemblies of stacked quartets possess a central channel, where the stabilizing ions are accommodated. The G-DNA stems are accompanied by single stranded loop regions joining the individual strands. Although the basic G-DNA motif based on the quartets looks simple, the G-DNA architectures are in reality extremely versatile,[1−8] and the diverse topological variants affect the dynamics of cation binding.[9,10]

G-DNA motifs can potentially form in different positions of the genome, including telomeric regions. Formation of G-DNA may take place during the DNA replication and transcription processes and can be associated with instability of the genome.[11] Therefore, G-DNA is of interest in anticancer treatment research.[12] More recently, G-quadruplex RNAs have been identified in regulatory regions of many mRNAs.[13−16] Last but not least, G-DNA is a potential scaffold for DNA-based nanostructures,[10,17] and its role in protein recognition by aptamers is under investigation.[18,19]

G-DNA structures have been subjected to intense experimental and theoretical investigations. The majority of theoretical studies on G-DNA involve molecular dynamics (MD) simulations that employ classical molecular mechanical (MM) force fields (FF),[20−46] including studies focusing on the ion dynamics inside the G-DNA.[20,47−52] Most common force fields that are employed in biomolecular simulations are additive, yet highly specific for classes of biomolecules such as nucleic acids and proteins, as a result of extensive parametrization against higher level ab initio quantum chemical (QM) data and experimental results. While the first MD studies on G-DNA molecules were executed on a time scale of a few nanoseconds, contemporary state of the art simulations are reaching a microsecond time scale.[53−56] MD simulations of G-DNA provided many valuable results, ranging from the basic characterization of structural dynamics of G-DNA molecules to insights into selected aspects of G-DNA folding that complement experimental data.[57,58]

Received: November 19, 2013
Published: February 3, 2014

   dx.doi.org/10.1021/ct4009969 | J. Chem. Theory Comput. 2014, 10, 1326−1340

Despite the success of many past G-DNA simulation studies performed using classical force fields, the simulations are affected by the overall simplicity and nonpolarizable nature of the force fields.[59] Indeed, several problems of the MM treatment of G-DNA molecules have been noticed. The first MD simulations revealed frequent formation of bifurcated H-bonding (inconsistent with X-ray data) for inner quartets in a G-DNA stem, as well as subtle discrepancies in positions of the internal G-DNA ions with respect to their experimental positions.[60] Both these findings were tentatively attributed to lack of polarization of the employed classical force field. Although these inaccuracies did not substantially disturb the simulations, they were early signs of potential imbalances in the MM description of G-DNA.

With increasing the simulation time scales, more serious problems emerged, mainly from exhaustive investigation of the conformational space of the *Oxytricha nova* dimeric quadruplex $d(G_4T_4G_4)$ with diagonal loops by means of MD, locally enhanced sampling (LES) MD and Poisson−Boltzmann surface area (MM-PBSA) free energy calculations. First, the simulations were unable to reproduce an experimental ion binding site at the stem loop junction.[61] It was suggested that this problem may reflect underestimation of the ion binding to the thymine loop residues. As will be shown below, the most likely origin of this discrepancy is different. In addition, the simulations were entirely unable to reproduce the native geometry of the four-thymidine loops (know from several independent X-ray and NMR studies). In long enough simulations, the native loop arrangements were irreversibly lost, while the MM-PBSA computations indicated that the force field indeed stabilizes non-native loop geometries. A similar problem was later reported for propeller loops of the parallel form of the human telomeric quadruplex DNA.[62] It thus appears that at least some G-DNA loops are difficult to describe by any existing variant of the force fields.

The lack of polarization in the force field can be illustrated by simple in vacuo comparison of MM and QM interaction energies between guanine's O6 atom and K^+ ion.[62] The MM interaction energies are visibly underestimated compared to QM, regardless of the MM parameters employed, while for short inter-atomic distances, the MM interaction energy curve rises more steeply and overestimates the short-range repulsion. Thus, the ions may look effectively oversized (too large) inside the G-DNA stem, which is consistent with the simulation results noted above.

More recently, MD simulations and MM-PBSA free energy computations were used to predict relative free energy stabilities of different topologies of G-DNA stems.[63] The calculations were in striking agreement with many experimental data, except that the stability of the all-parallel all-*anti* G-DNA stem appeared to be systematically underestimated compared to the antiparallel quadruplexes. Subsequently, the different G-DNA stem topologies were also assessed using large-scale QM DFT-D3 computations.[64] These computations revealed a sizable difference between QM and MM descriptions of the relative energies of parallel and antiparallel G-DNA stems, which has been primarily attributed to the description of the backbone.[65] Using the QM calculations as correction to the earlier MM-PBSA simulation data made the prediction consistent with the experiments.

The capability of MM force fields to describe G-DNA molecules was recently addressed by Song et al.[66] These authors developed a specific modification of the Cornell et al. MM model[67] for the MD simulation of the *Oxytricha* quadruplex termed the "polarized nucleic acid-specific charge (PNC)" model. It includes polarization effects by specifically deriving charges exactly for the studied quadruplex molecule. The subsequent simulations were successful both at describing the ion positions in the structure and at maintaining the correct H-bonding pattern among the bases, at least on the given simulation time scale. Although a force field parametrized in this manner is not easily transferable to other systems or even to other arrangements of the same molecule, the limitations of the common force field description are nicely visualized.

It is undeniable that past MD simulations provided important insights into G-DNA structural dynamics and interactions. However, with continuous hardware and software developments, the simulations are becoming longer and longer. The improved sampling allows substantial broadening of the spectrum of computations that can be carried out for G-DNA. However, at the same time, the results are getting more and more sensitive to approximations of the force field, leading to accumulation of errors along the trajectories. For example, any studies attempting folding of G-DNA will be sensitive to the force field performance. Therefore, it becomes tempting to scrutinize in detail the actual performance of MM force fields for G-DNA (and in general for all classes of nucleic acids) in order to understand limitations of the simulation technique and eventually to improve its performance.

An important approach to understand the force field approximations is to compare MM results with QM results. Actually, numerous examples of QM studies are available[21,68−77] that deal with several aspects of G-DNA architectures. For example, G-quartets have been shown to be more stable than adenine quartets.[68] Stacking arrangements of the former, with K^+ as coordinated ion, have been extensively investigated by ab initio and MM methods, showing an overall satisfactory agreement between the two levels.[21] Additionally, the selectivity of G-quartets for K^+ over Na^+ has been probed by various methods.[69,71,75,77] Other studies on ion binding to G-quartets have shown that quartets with small ions with high charge are more likely to be nonplanar, in contrast to Na^+ and K^+, and that charge transfer from the quartets to the metal ions occurs.[73] An extensive study including DFT and HF potential energy surface (PES) calculations, along with NMR parameters and vibrational frequency calculations, has shown the energy minima that occur for Li^+, Na^+, and K^+ penetration into stems of various quartet−quartet separations, among other findings.[74] The same study also examined the energetic barriers for penetration of these ions into the stem, showing that the largest barrier occurs for K^+. Finally, the H-bonding pattern and cooperativity have been addressed.[70,72,74]

The present study investigates the accuracy of MM description of binding of ions to the G-DNA stems, an issue that has not yet been systematically addressed in the QM literature. Our study builds upon recent advances in development of fast and accurate QM methods, which allows studies of larger systems (almost 200 atoms in our case) using QM methods. We investigate the origin and magnitude of the discrepancies between the QM and MM levels using idealized models of two and three guanine quartet arrangements with one and two ions (using Li^+, Na^+, and K^+) both in the gas phase and in implicit solvent. We performed a series of PES scans, similar to those of ref 74, in which the ion starts from a position in close proximity to one of the quartets and is gradually inserted toward the center of the stacked quadruplex model

through the guanines carbonyl oxygen channel. The computations reveal large and hitherto unnoticed differences between QM and MM descriptions of binding of multiple ions to the G-DNA stems, which may explain several of the unsatisfactory simulation results noted above.

METHODS

Preparation of Reference Geometries. Four optimized guanines were used to form a planar quartet with C_{4h} symmetry, which was subsequently optimized (without the ion) conserving the symmetry at the B3LYP/6-31G(d,p) level. This optimized quartet has a cavity size somewhere between the sizes that would be optimal for Na^+ and K^+ ion binding (see below) and is thus suitable for the PES scans. Stacked systems were initially prepared by placing the optimized quartets at an ideal distance of 3.4 Å with a helical twist of 45° between them (Figure 1) without further optimization at the QM or MM levels. It should be noted that keeping the geometries fixed is obviously an approximation. However, we suggest that it is entirely valid to assess the qualitative difference between MM and QM descriptions of binding of multiple ions to the G-stems, which is the main focus of our work. Making relaxation of the quartets would complicate the computations by adding several additional degrees of freedom to consider and, strictly speaking, would have to be done individually for each quartet and for each ion position. We have used both possible mutual orientations of the quartets, namely, the same orientation and the opposite orientation (Figure 1). The ion(s) were placed in positions along the C_4 axis of the stacked quartets. The exact positions of the ions for each PES scan are explained in the Results and Discussion section, together with eventual adaptations of the quartet geometries. In all cases, the guanine quartets are perpendicular to the *z*-axis, and the ions move along the *z*-axis.

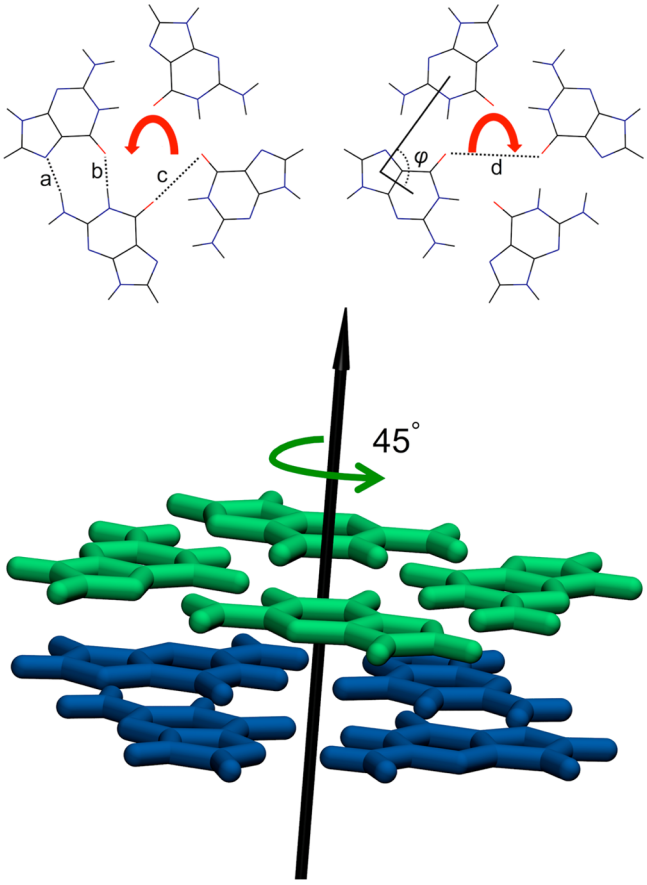

Figure 1. Top: Geometry of the quartets. H-bonds and O−O distances are denoted as a, b and c, d, respectively. The angle φ corresponds to the angle formed by the line connecting the 6- and 5-member ring centroids of one guanine and the 6-member ring centroid of its adjacent guanine. The red arrows indicate two possible orientations of the quartets. Two consecutive quartets in the stem can have either the same or opposite orientation.[21,64] Bottom: Schematic representation of the stacked arrangement of same orientation quartets with a helical twist of 45°. (Helical twist of stacked quartets with opposite orientation is displayed in Figure S1 of the Supporting Information.)

High-level (QM) energies were evaluated using the TPSS[78] meta-GGA functional enhanced by Grimme's latest London dispersion correction (D3) with Becke−Johnson damping[79,80] and the sufficiently large def2-TZVP[81,82] all electron Gaussian AO basis set. An *m*4 grid was used for evaluation of the exchange-correlation integrals and the resolution of the identity (RI) approximation[83,84] for the two-electron Coulomb integrals. All calculations were performed using the ORCA package[85] (version 2.9.1), apart from the quartet geometry optimizations, which were performed using Gaussian09 (Revision D.01).[86] For continuum solvent calculations, the COSMO continuum solvation model[87−89] is employed, with a dielectric constant of 80.4. The atomic radii for the cavity construction were kept at their software defaults, which are (in Å) C, 2.0; N, 1.83; H, 1.3; O, 1.72; K, 2.22; Li, 1.40; and Na, 1.75. Gas-phase and COSMO calculations are abbreviated as QM(gas) and QM(COSMO).

All MM energies were calculated using the AMBER12 package.[90] The Cornell et al. force field[67] was employed for description of the guanine molecules. The hydrogen atom bonded to the N9 atom was assigned a charge of 0.089 e to neutralize the molecule, while all other atoms were described by their original MM charges. The 2008 Young and Cheatham ion parameters for TIP3P water were used for the description of the cations.[91] Both MM gas phase (MM(gas)) and MM with implicit solvation calculations were performed without periodic boundary conditions and without cutoffs. Implicit solvation calculations were performed using the generalized Born/surface area (MM-GBSA) and Poisson−Boltzmann surface area (MM-PBSA) approaches, excluding the surface area term. The former were performed using the Hawkins, Cramer, Truhlar model[92,93] with the default parameters[94] and radii, as implemented in AMBER12. The latter were performed with the level set function implementation for the dielectric interface. To achieve sufficient accuracy, the MM-PBSA calculations employed a grid spacing of 0.2 Å. All other functional parameters of the MM-GBSA and MM-PBSA were kept to their software default values, unless otherwise stated.

Additional calculations on selected systems were performed at the symmetry-adapted perturbation theory (SAPT) level using the PSI4 package.[95] Because of the large size of the systems, the SAPT0 approximation was employed using the natural orbital implementation of Hohenstein[96] combined with a density-fitting scheme.[97,98] As suggested by the authors, the jun-cc-pVDZ basis set for SAPT0 was used that partially relies on error compensation. It is a variant of the aug-cc-pVDZ[99−101] basis set with a reduced number of diffuse functions (formerly denoted aug-cc-pVDZ′).[98] The jun-cc-pVDZ basis set and corresponding auxiliary basis sets of Al were used for Na. This

Table 1. H-Bond (a, b), O−O (c, d), and Cation−O (X−O6) Distances, Guanine−Guanine Angles (φ), and Cation−Quartet Interaction Energies (E_{int}, neither quartet relaxation nor monomer deformation energies are included) of Optimized Quartets with and without Ions the at QM (TPSS−D3, B3LYP) and MM Levels

	a (Å)	b (Å)	c (Å)	d (Å)	X −O6 (Å)	φ (degrees)	E_{int} (kcal/mol)
					quartet−no ion		
B3LYP[a]	1.97	1.78	3.50	4.94	−	89.0	−
TPSS−D3	1.97	1.73	3.43	4.85	−	89.0	−
MM	2.51	1.89	4.07	5.75	−	79.8	−
					quartet−K^+		
B3LYP	2.08	1.95	3.59	5.07	2.54	90.6	−78.7
TPSS−D3	2.04	1.89	3.58	5.07	2.54	90.0	−78.8
MM	2.13	1.95	3.59	5.08	2.54	96.7	−69.8
					quartet−Na^+		
B3LYP	1.89	1.87	3.24	4.59	2.29	92.6	−116.8
TPSS−D3	1.85	1.82	3.24	4.58	2.29	92.1	−111.7
MM	1.95	2.02	3.19	4.51	2.25	93.3	−106.3
					quartet−Li^+		
B3LYP	1.80	1.85	3.03	4.29	2.15	93.8	−144.2
TPSS−D3	1.76	1.81	3.01	4.26	2.13	93.6	−139.1
MM	1.93	2.33	2.78	3.94	1.97	99.7	−157.5

[a]This quartet geometry has been used to perform all QM and MM scans of the ion binding in this study, unless stated otherwise.

basis set is slightly larger than necessary and not optimized, but because Na JK-fitting basis sets for aug-cc-pVDZ are not available, it is the simplest practical solution that provides reliable results. Systematic errors caused by the suboptimal basis set should cancel out because we are primarily interested in relative energies.

We also report preliminary data derived from the quantum theory of atoms-in-molecules (QTAIM)[102] by analyzing the topology of the density and integrated atomic properties of selected systems. QTAIM calculations were performed with the AIMAll software.[103]

RESULTS AND DISCUSSION

In this work, we assess differences between the MM and QM descriptions of binding of one and two ions to G-DNA and G-RNA (G-NA) stems represented by two or three G-quartets. In case of the binding of one ion, the lack of polarization in the MM description may affect the direct (primary) ion binding to the G-quartets. The interactions become even more complex in the case of binding of two ions because the inter-ion repulsion inside the G-stems, and its attenuation by the G-quartets may be described differently by the QM and MM methods. Eventual differences, if significant, would be transferred to explicit solvent simulations and affect their outcomes.

We separately discuss the gas-phase and continuum solvent results. The continuum solvent data are closer to the real nucleic acids systems but can be affected by differences and inaccuracies of the solvation models. The gas-phase data give unambiguous insights into the intrinsic difference between the MM and QM descriptions of the ion binding; however, they can also exaggerate trends associated with long-range electrostatic effects compared to the water environment relevant to nucleic acids. For balanced evaluation of the differences, both pieces of data should be considered.

Geometry of Quartets. A single planar quartet was optimized in gas phase, both at the QM and MM levels, with preservation of the symmetry. The geometric parameters a−d and φ (Figure 1) are displayed in Table 1. We used the distance (c) between the carbonyl oxygens of two adjacent guanines as a primary measure of the cavity size. The interaction energies (E_{int}) displayed in Table 1 are between the quartet as one subsystem and the ion as the second subsystem, i.e., pure ion−quartet inter-molecular terms. Thus, no guanine−guanine interactions are included, which could possibly modulate the interaction energy differences between the QM and MM methods. However, our main analyses include relative energies along scans of ion movement with fixed stem geometries. Therefore, differences in guanine−guanine contributions cancel each other for all calculations present in this study.

On the basis of the QM data, the cavity size varies from 3.03 to 3.50 Å and is in agreement with previous estimates.[73] The QM cavity size follows the order Li^+ < Na^+ < no ion < K^+. MM optimizations resulted in a larger cavity size when no ion is present than when a K^+ is present. MM shows, in the absence of an ion, formation of bifurcated H-bonds, as those first observed in ref 60, which have also been observed in calculations with the MMFF94 force field.[73] This can be seen by the large distance of the N−H···N hydrogen bond (a = 2.51 Å). Starting from this MM geometry, QM optimization resulted in the nonplanar bifurcated quartet structure of S4 symmetry that has been reported before.[68] However, with the modern DFT-D3 method, the bifurcated structure is approximately 3 kcal/mol less stable than the QM planar geometry, so we concluded that the planar geometry is relevant for our study. Additionally, nonadditivity effects[104] are more intense in the presence of the ions, resulting in shortening of the H-bonds at the QM level,[75] which is not the case at the MM level. Nevertheless, considering all data, the differences between QM and MM descriptions for the Na^+ and K^+ binding are not large, and due to compensation of errors, they should not be a concern for explicit solvent simulations.

On the basis of the results, we selected to perform the scans using the QM-optimized quartet structure without ions, as its cavity size is intermediate between the K^+ and Na^+ cases, being closer to the K^+-bound quartet than to the Na^+-bound quartet (as judged by the distance "c"). MM and QM geometries are in good agreement for Na^+ and K^+-bound quartets, while there is a larger difference in case of Li^+ binding.

Binding of One Ion to Two Quartets. The first PES scan was performed for one K^+ ion and two quartets (two-quartet

dx.doi.org/10.1021/ct4009969 | J. Chem. Theory Comput. 2014, 10, 1326−1340

stem) using both the same and the opposite orientation arrangements of the quartets. The K^+ ion was gradually pushed to the center of the inter-quartet cavity, starting at a distance of 1.7 Å away from the plane of the closer quartet (Figure 2). The

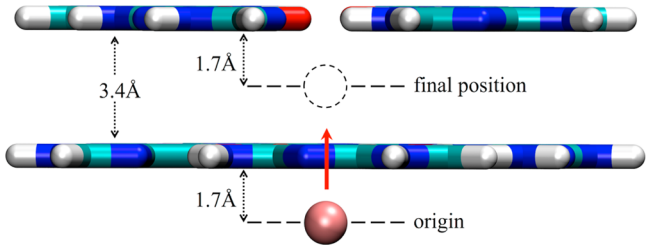

Figure 2. Schematic representation of the one-ion/two-quartet PES scans.

PES scan was evaluated for motion of the ion along the *z*-axis with 0.2125 Å step, and the starting position was taken as the reference point (Figure 3). The results are unaffected by the

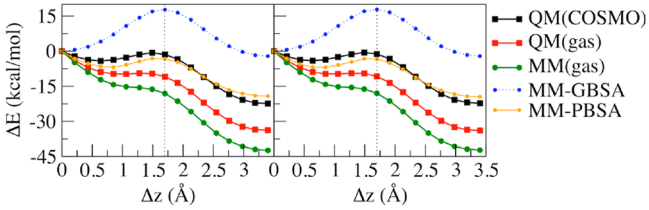

Figure 3. PES curves for the one-ion/two-quartet system with K^+ and considering the same (left) and opposite (right) relative quartet orientations. Δz is distance of the ion from the starting position; the individual points are separated by 0.2125 Å steps. The vertical line marks passage of the ion through the quartet plane (Figure 2). Figure S3 of the Supporting Information displays the same data using the ion position in the cavity center as the reference point. Exact ion coordinates are included in Tables S1 and S2 of the Supporting Information.

relative orientation of the quartets with differences between the two quartet arrangements not exceeding 0.2 kcal/mol. We have therefore made most subsequent calculations in this study only with the arrangement having the same orientation of the quartets.

It should be noted that both QM and MM scans are done with the same stem geometries based on B3LYP optimized empty quartets. Obviously, different ions have different optimal cavity sizes, and there is also a difference between optimal cavity sizes at the QM and MM levels of description (Table 1). These circumstances may affect to a certain extent the calculated PES scans. However, in all cases when we analyze the differences between the QM and MM descriptions, we report qualitative differences that should not be affected by our specific stem geometry choice. The reader should also take into consideration that we typically show energies with respect to a reference point where the ion is outside the stem in close contact with the proximal quartet. This is because we are primarily interested in investigating the QM vs MM energy difference of the biochemically relevant process of ion penetration into the stem. In Table S1 of the Supporting Information, we also present energies with respect to the ion being infinitely separated from the stem.

QM and MM Data Show Modest Gas-Phase Energy Difference for Binding of a Single Ion to the Stem. Let us first discuss the gas-phase trends, i.e., the red (reference QM) and green (MM) curves. While the MM(gas) and QM(gas) curves show similar qualitative trends, the MM(gas) relative energies are consistently lower with increasing difference from the respective QM(gas) data as the ion approaches the two-quartet system. While the ion is located outside the cavity (for $\Delta z < 1.7$ Å in Figure 3), the MM(gas)−QM(gas) difference gradually rises up to almost 7 kcal/mol. The MM ion-binding curve is more stabilizing. At $\Delta z = 1.7$ Å, the ion passes through the quartet plane, and beyond that point, the difference between the MM and QM energies (relative to the starting point, Figure 3) stabilizes at 8.0−9.0 kcal/mol.

The calculations predict that the ion binding event is more stable at the MM level than at the QM level, which is somewhat counterintuitive. At first sight, we would expect that MM should underestimate the energy gain from the ion binding due to lack of stabilizing polarization energy. We have carried out series of computations to resolve this point (Supporting Information). First, because the AMBER force field uses HF ESP (electrostatic potential) charges that overestimate the guanine dipole moments,[67] we have repeated the MM calculations with MP2 ESP charges. However, the results are unchanged. Then, we repeated the PES scans with fragments of the proximal quartet, namely, with a single guanine, two adjacent guanines, two oppositely placed guanines, a guanine triad, and finally, the full quartet (Figure S2, Supporting Information). The QM(gas) is more stabilizing than the MM(gas) when binding the ion to single guanine, two guanines, and a guanine triad. However, the energy difference is reduced with the number of guanines. The trend is reversed, and the MM becomes more stabilizing when the ion interacts with the complete quartet. Closer examination of the observed trends reveals the origin of this behavior. Each guanine that is added to the system causes additional stabilization of the ion binding. In the case of MM method having no polarization, this additional stabilization is additive, being approximately −4 kcal/mol per guanine (with respect to the starting point). In contrast, using the QM description, there is a gradual decrease in the additional stabilization by adding the additional guanines. While binding of the ion to the single guanine brings almost −6 kcal/mol stabilization, the binding of the ion to G-triad and G-quartet is essentially isoenergetic (Figure S2 and Table S3, Supporting Information). We suggest that the effect is analogous to the well-known mounting polarization inter-ligand repulsion with increasing the number of the ligands in the cation coordination shell.[105−107] We re-emphasize that the guanine and ion are kept in their positions as depicted in Figure 2, and we report relative energies with respect to the starting ion position and not with respect to the infinity. The ion is off the plane of G and approaches the guanine in a direction vertical to the C═O vector. Thus, the 6 kcal/mol stabilization reported above is smaller in magnitude than the binding energy of a monovalent cation to a guanine base calculated with respect to the infinitely separated monomers.

GBSA Continuum Solvent Model Deviates Considerably from COSMO and PBSA Data When the Ion Is Outside the Stem. The MM-GBSA data are in clear disagreement with the MM-PBSA and QM(COSMO) data. The latter two methods show overall qualitative similarities both with each other and with the gas-phase data. Both predict a shallow local minimum for the ion located outside the stem at a distance of 0.85−1.0625 Å from the proximal quartet and a small barrier at 0.2125 Å before the ion reaches the proximal

quartet's plane. On the other hand, the MM-GBSA data predict a much higher barrier for insertion of the ion into the cavity that reaches almost 18 kcal/mol at the plane of the quartet. Note that the difference is exclusively due to geometries with the ion outside the stem. When the ion moves inside the stem, the shape of the MM-GBSA energy curve agrees with the other two continuum solvent methods.

Continuum Solvent Eliminates Gas-Phase Energy Difference between QM and MM Descriptions. To unambiguously assess the continuum solvent data is more difficult because there are large differences between the continuum solvent models. It is not easy to a priori tell which of the common continuum solvent models is better. Further extensive testing would be necessary to reach solid conclusions, but this is outside the scope of the present work. The results illustrate uncertainty in continuum solvent calculations of nucleic acids with the commonly used methods. Nevertheless, the most important result is that when using the COSMO and PBSA methods, the continuum solvent essentially eliminates the difference between the QM and MM energy scans.

Effect of Quartet Size. To estimate the effect of quartet size, additional calculations were performed in which one quartet and the K^+ cation were kept fixed in space, while the second quartet was gradually opened by shifting each of the four guanines along the $\pm x$ and $\pm y$ directions with 0.1 Å steps (Figure S4, Supporting Information). This shift corresponds to an increase in the neighboring and opposite O atoms distance of approximately 0.09 and 0.14 Å per step, respectively. The cation was kept fixed at the center of the cavity. The trends of the energy changes, ΔE, with respect to the initial geometry are shown in Figure 4 (left) and in Table S4 of the Supporting Information. The calculations reveal only a small difference between the QM(gas) and MM(gas) data. This indicates that MM should correctly capture small fluctuations of the G-quartets (which obviously take place during explicit solvent simulations), which in turn hints at small perturbations of the electronic charge distribution of the system upon such quartet fluctuations. Importantly, the MM-PBSA, QM(gas), and MM(gas) methods show insignificant mutual differences (below 0.5 kcal/mol), while the QM(COSMO) data are still very close to them. This particular calculation does not indicate any major MM discrepancy that would affect the simulations. It also justifies our approach using rigid quartet systems in our computations. The MM-GBSA data again deviate from the other methods.

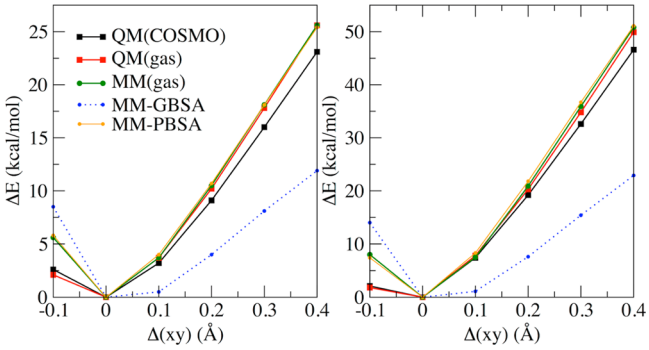

Figure 4. PES scan for "opening" one (left) and both (right) quartets in the one-ion/two-quartet (same orientation of the quartets) system with the K^+ cation fixed at the center of the cavity.

For the sake of completeness, the energetics of the cavity size change show larger dependence on the relative orientation of the quartets (same orientation vs opposite orientation) than that observed for the ion insertion scan. However, the differences do not exceed 1 kcal/mol (Table S4, Supporting Information), which we still consider as negligible.

Opening of both quartets in the same manner leads to equivalent results. The variations of the relative energies are almost doubled (Figure 4 (right) and Table S5, Supporting Information), as expected for opening both quartets. However, the differences among the methods maintain the pattern described above.

Scans with Na^+ and Li^+. In order to examine the effect of the cation type (size), the PES scan described in Figures 2 and 3 was repeated with Li^+ and Na^+ (Figure 5 and Table S6, Supporting Information). The ion insertion is evaluated using the same quartet geometry as for K^+ (kept fixed to a model geometry optimized without ions). Thus, on then basis of the data presented in Table 1, the quartet size is now larger than the optimal for these two ions. All main differences between Figures 3 and 5 may be rationalized on this basis.

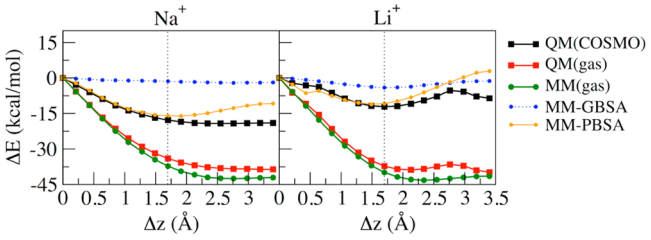

Figure 5. PES curves for the one-ion/two-quartet system (Figure 2) with Na^+ (left) and Li^+ (right) ions. The vertical line marks passage of the ion through the quartet plane. Exact ion coordinates are included in Table S6 of the Supporting Information.

Figure 5 reveals similar, albeit somewhat smaller, gas-phase differences between the QM and MM descriptions as seen for K^+ in Figure 3. As the ion approaches the stem, the MM gas-phase curve becomes overstabilized by 3.0−6.0 kcal/mol and 3.0−4.5 kcal/mol for Li^+ and Na^+, respectively, compared to the QM data. MM-GBSA data remain in notable disagreement with the other methods. As Na^+ and Li^+ are smaller, the barrier for ion passage through the quartet shown in Figure 3 disappears in Figure 5. Additionally, a bump is observed in both QM curves for Li^+ inside the stem. It likely reflects the imbalance between the ion size and quartet size. Specifically, the Li^+ quartet complex is known to be more stable at S4 symmetry.[73] The difference between solvation and gas-phase curves is larger than that observed for K^+, especially for the smallest Li^+ ion.

Keeping the quartets fixed in space enables us to examine the effect of changing the ion type while having identical stem geometries. A potential limitation of this approach is that the cavity is not relaxed to its optimal size for each ion, in contrast to ion dynamics in real systems and in MD simulations. Therefore, we repeated the scans for all ions with the B3LYP optimal cavity radius that corresponds to smaller Na^+ (Table 1). The scans and detailed data are presented in Figure S5 and Table S7 of the Supporting Information and should be compared with Figures 3 and 5 in the main text. Briefly, the

dx.doi.org/10.1021/ct4009969 | J. Chem. Theory Comput. 2014, 10, 1326−1340

data show that using this quartet size would lead to identical conclusions about the QM vs MM differences as obtained from the original calculations given in Figures 3 and 5. Specifically, for Na^+ and Li^+, we found no noticeable differences except that the energy slopes are larger. This corresponds to a larger energy gain of the ion penetration into the cavity center. These two ions experience larger stabilization inside the stem because the smaller cavity radius fits better these two ions, and in addition, the guanines are now closer to each other, creating more negative pocket of electrostatic potential in the stem. Importantly, the differences among the different methods remain the same as discussed above for the original scans in Figures 3 and 5.

The only difference is that this quartet size is now evidently too small for K^+, as expected. This gives rise to a considerable energetic barrier for K^+ penetration into the stem (i.e., when the ion passes through the quartet plane). The barrier is approximately 4 and 12 kcal/mol at the QM(gas) and QM(COSMO) levels, respectively. This energy barrier is almost doubled at the respective MM(gas) (8 kcal/mol) and MM-PBSA (23 kcal/mol) levels. This indicates a very severe steric clash between the K^+ ion and the smaller quartet once the ion is in its plane. The force field Lennard–Jones spheres do not describe this steric clash satisfactorily, that is, the force field approximation becomes quite inaccurate in this steric clash region. This, however, is not of a concern. This geometry is not relevant for simulations because the quartet would respond by enlarging its size due to the energy gradient associated with such a clash. Importantly, when we exclude data points with close contact between the K^+ ion and the quartet, QM-(COSMO) and MM-PBSA data are in very good agreement again. In summary, changing the size of the quartet does not change any of our analyses of the QM vs MM difference obtained in the first set of calculations. We did not repeat the calculations with the quartet size adapted to Li^+ because for such small cavity the K^+ scan would become even more unrealistic.

Additionally, a series of scans were performed for all ions with expanded cavities (as described above). Again, only small differences between the QM and MM levels are observed (Figure S6, Supporting Information).

Expected Effect of MM Approximation on MD Simulations. The above results suggest the following consequences for classical MD simulations. Although Figures 3 and 5 show a rather visible difference in the ion binding MM and QM curves in the gas phase, the difference is attenuated when applying the PBSA and COSMO solvation models. So, we suggest that the one-ion/two-quartet energy scans do not indicate any major bias of the simulations for the binding of one ion to the G-stem. It does not mean we suggest that the MM description is perfect, but we assume that due to compensation of errors the MM description of this process is fairly acceptable. The surprising difference between PBSA and GBSA computations should be considered if ion binding to G-NA stems is studied by continuum solvent computations. Further analysis of this difference is beyond the scope of the paper.

Binding of One Ion to Three Quartets. We have repeated the PES scan for one ion with three stacked quartets. The step of the ion movement is doubled to 0.425 Å, starting from the same distance outside the stem as for the two-quartet case and ending at equal distance outside the second cavity (Figure 6). The results (Figure 7 and Table S8, Supporting Information) show straightforward extension of the data with

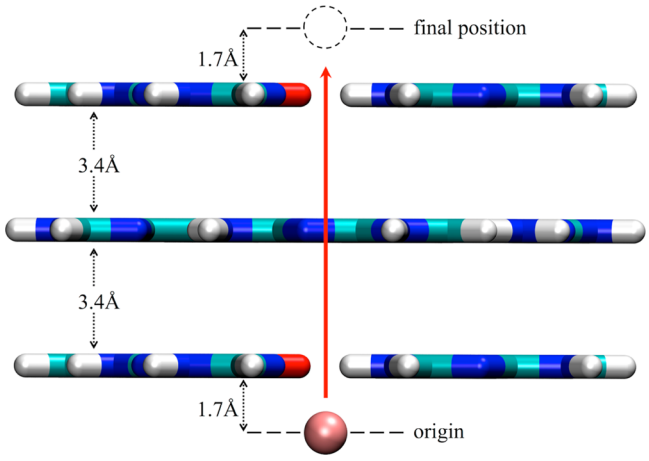

Figure 6. Schematic representation of the one-ion/three-quartet PES scans.

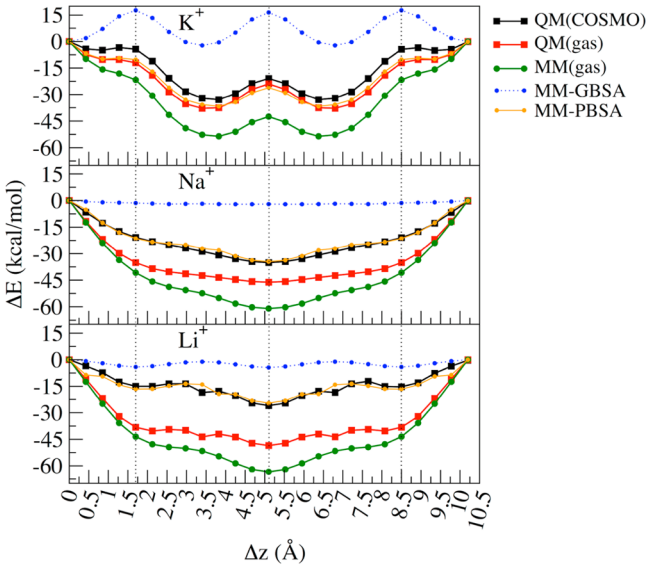

Figure 7. PES curves for the one-ion/three-quartet system with K^+ (top), Na^+ (middle), and Li^+ (bottom) ions. Δz is the distance of the ion from the starting position; the individual points are separated by 0.425 Å steps. The vertical lines mark passage of the ion through the quartet plane. Exact ion coordinates are included in Table S8 of the Supporting Information.

one ion and two quartets. The K^+ ion faces a barrier for passing through the middle quartet, while the smaller Na^+ and Li^+ ions are stabilized at the plane of the middle quartet. This result is obviously specific for the given quartet size that we use. The stabilization is stronger for Li^+, which can more easily be accommodated in the plane of the quartet due to its smaller size.

The gas-phase differences between the MM and QM data somewhat increase upon including the third quartet. The maximum differences between the QM and MM gas-phase data is approximately 15 kcal/mol for Li^+ and Na^+, respectively, while for K^+, the maximum difference reaches up to 18.5 kcal/mol. However, inclusion of the solvent via COSMO and PBSA eliminates the difference between the QM and MM calculations, indicating that we may expect good performance of the force field in simulations. The GBSA calculations

dx.doi.org/10.1021/ct4009969 | J. Chem. Theory Comput. 2014, 10, 1326–1340

resemble those discussed for the one-ion/two-quartet stem and differ dramatically from the PBSA data.

Binding of Second Ion to Two-Quartet Stem Reveals Large Overestimation of Inter-Ion Repulsion at the MM Level of Description. The above data with one ion suggest that perturbations of the charge distributions when a single ion moves into the G-stem are responsible for the difference between QM and nonpolarizable MM descriptions. Obviously, other factors can contribute such as short-range effects or change of coordination between the cations and the O6 oxygens as the ion changes position near or inside the stem. These effects can be captured by the MM formalism only approximately. However, as we explained above, the QM vs MM energy differences for binding of a single ion can be considered as rather small and are reduced by solvent screening. Thus, due to compensation of errors, they should not affect MD simulations dramatically. However, a more biologically relevant scenario is binding of multiple ions to the G-stems. The accuracy of description of binding of multiple ions could be affected by the inter-play between increased polarization effects and cation−cation repulsion.

We examined interactions of two cations with a two-quartet stem (Figure 8). One ion was kept fixed (the upper one in the

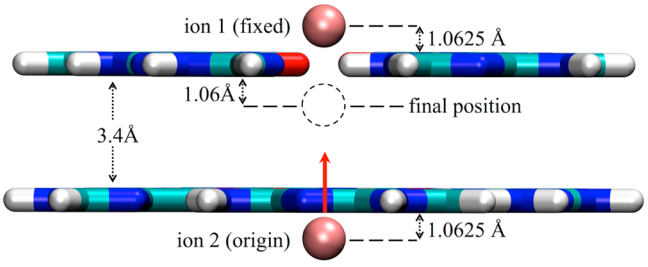

Figure 8. Schematic representation of the two-ion/two-quartet PES scans.

Figure 8), and the second ion was gradually inserted into the stem. Both ions are initially positioned outside the stem each at 1.0625 Å from the adjacent quartet. The initial position was selected based on the PES scans shown in Figure 3, revealing a local minimum at approximately this distance.

The results are very different from those in Figures 3 and 5. All curves show a steep energy increase as the distance between the ions decreases, reflecting the inter-cation repulsion (Figure 9 and Table S9, Supporting Information). There is a striking difference between the QM and MM gas-phase energy curves that increases with reducing the inter-ion distance. It is much more endoergic to move the ion into the stem at the MM level than at the QM level. The effect is similar for all ions and starts when the ions are still well separated, so it is not due to van der Waals interaction. When comparing the position of the moving ion within the plane of the quartet (Δz = 1.0625 Å) and in the center of the cavity (Δz = 2.55 Å), the energy differences between QM and MM data increase from 4.0 to 21.0, from 8.0 to 24.5, and from 6.0 to 25.0 kcal/mol for K^+, Li^+, and Na^+, respectively. The results are fully confirmed when repeating the calculations with the smaller quartet cavity size that corresponds to Na^+ (Figure S7 and Table S10, Supporting Information).

Expected Effect of MM Approximation on MD Simulations. Importantly, this sizable difference between QM and MM descriptions is not compensated for by the

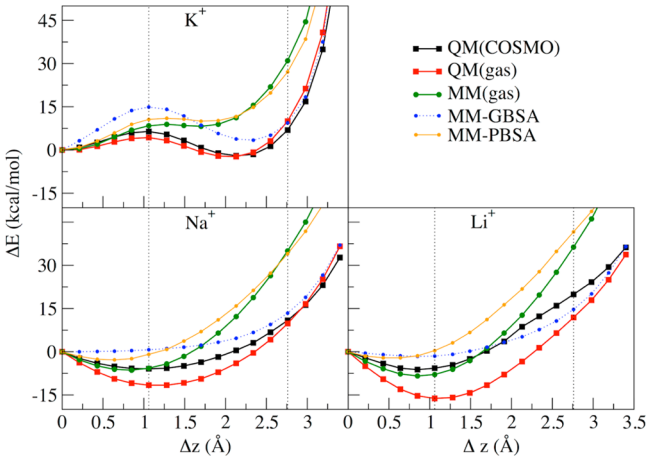

Figure 9. PES curves for the two-ion/two-quartet system with K^+, Na^+, and Li^+ ions. Left and right vertical lines mark the plane of the first quartet and the cavity center, respectively. Exact ion coordinates are included in Table S9 of the Supporting Information.

continuum solvent and thus is assumed to bias ion dynamics and binding in explicit solvent simulations (Figure 9, black and yellow curves). In other words, contemporary MD simulations are likely affected by a rather large overestimation of the inter-cation repulsion inside G-NA molecules. We expect that the following inaccuracies bias the simulations: (i) slow down of binding of the ions to the G-stems in simulations compared to real systems, (ii) biased dynamics of multiple ions inside the stems, and (iii) inadequate (excessive) expulsion of ions from the stems and stem−loop junctions. These inaccuracies should be considered in all force field studies analyzing ion movements in the G-NA stem and ion binding. Both structural dynamics and free energies are assumed to be affected. Our observation explains the notoriously observed loss of the ions from the stem−loop junctions in simulations of the $d(G_4T_4G_4)_2$ diagonal loop quadruplex.[61] The stem−loop ions are expelled from the structure due to unrealistic (excessive) inter-cation repulsion with the proximal stem ions.

We suggest that the physical chemistry explanation of the effect is as follows. At the QM level, there is a large polarization interaction between the ions and the quartets. This effectively softens or compensates for the electrostatic inter-cation repulsion, that is, the quartets help to screen the inter-cation repulsion. At the pair-additive MM level describing ions with fixed point charge +1, the inter-cation repulsion is exaggerated. (Further, as the ions approach each other, the net charge sensed by the guanines is increased or more concentrated, leading to larger polarization energy.)

At first sight, the MM performance could be improved by some reduction of the charge of the ions. However, such charge reduction would have to be severely geometry-dependent and thus cannot be done within the constant point charge model (see below).

Binding of One Ion to Three Quartets with Second Ion Present. To confirm the results, we repeated the two-ion calculation with three stacked quartets (Figures 10 and 11 and Table S11,Supporting Information). The fixed ion is located at the center of one cavity (top, Figure 10). The second ion starts from a distance of 1.7 Å outside the stem and is gradually inserted into the center of the second cavity. The overall trends are similar to those with two quartets, taking into account that the fixed ion is shielded in the cavity rather than exposed in the

dx.doi.org/10.1021/ct4009969 | J. Chem. Theory Comput. 2014, 10, 1326−1340

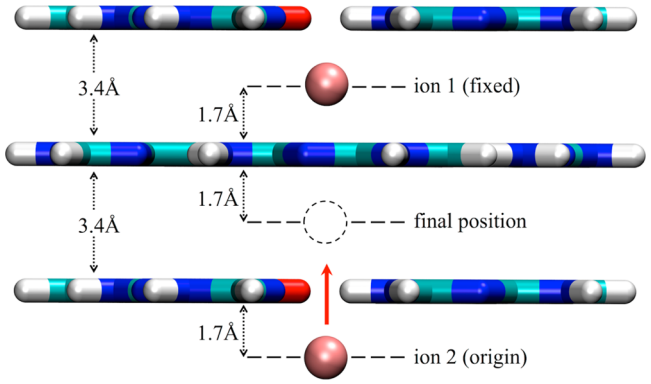

Figure 10. Schematic representation of the two-ion/three-quartet PES scans.

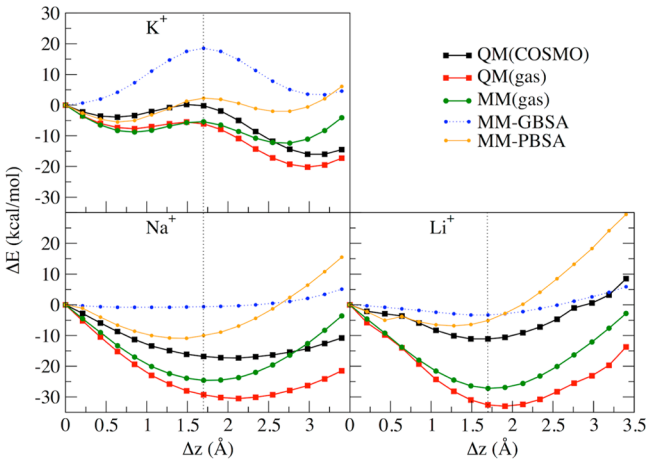

Figure 11. PES curves for the two-ion/three-quartet system with K^+, Na^+, and Li^+ ions. The vertical line marks passage of the ion through the quartet plane. Exact ion coordinates are included in Table S11 of the Supporting Information.

vacuum or the implicit solvent environment. For the PES portion with the ion already moving inside the stem, the gas-phase QM vs MM (red vs green curves) difference increases from approximately 0.5 to 13.0, from 5.0 to 18, and from 5.5 to 11.0 kcal/mol for K^+, Na^+, and Li^+, respectively. The calculations fully confirm the results obtained for the two-ion/two-quartet systems, namely, large overestimation of the inter-cation repulsion by the nonpolarizable MM. The difference is not eliminated upon inclusion of the solvent via the COSMO and PB approaches (black vs yellow curves).

For completeness, we have also calculated the ion−ion repulsion in absence of the quartets (Figure S8, Supporting Information). As expected (because there is no modulation of the ion−ion interactions by the guanines), the QM and MM descriptions mutually agree, and the fixed point charge description works well. The QM vs MM difference in the description of the inter-cation repulsion arises only in presence of the G-NA structure.

Movement of Two Ions with Fixed Distance through Three-Quartet Stem. We have performed an additional scan by moving the two K^+ ions as a rigid entity along the path shown in Figure 12. This keeps the ion−ion distance constant, while varying the interaction of the cation couple with the quartet system. Note that all sampled geometries have a rather significant degree of ion−quartet interactions (Figure 12). By

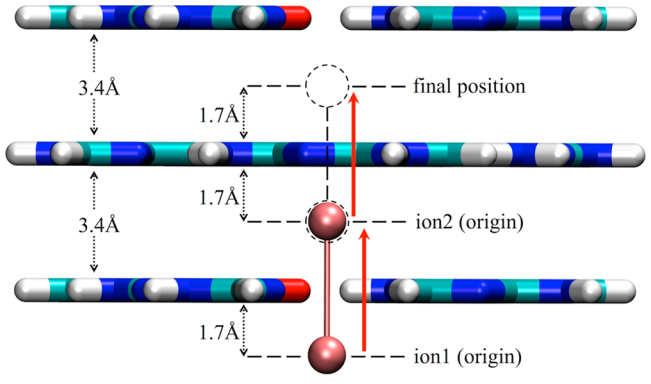

Figure 12. Schematic representation of the two-ion/three-quartet PES scans with the two ions treated as a rigid block (simultaneously).

keeping a constant inter-cation distance, we do not visualize the effect of an incorrect description of the ion−ion repulsion (i.e., it affects the curves only implicitly, as a "second-order" effect). The PES curves (Figure 13 and Table S12, Supporting

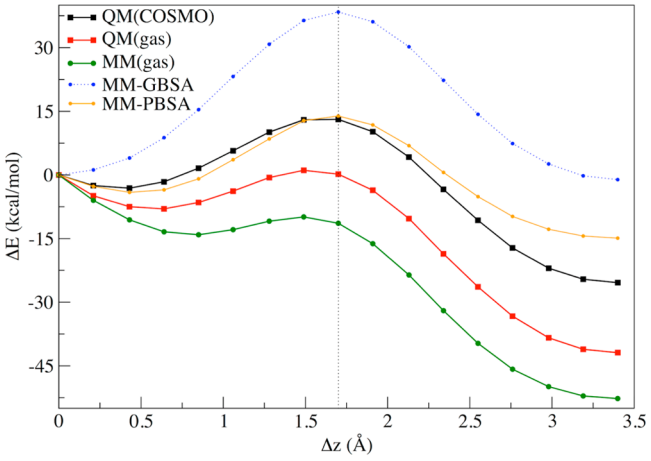

Figure 13. PES curves for the two-ion/three-quartet system with the two K^+ ions treated as a rigid block. The vertical line marks passage of the ions through the quartet planes. Exact ion coordinates are included in Table S12 of the Supporting Information.

Information) show differences that exceed 10 kcal/mol between the QM and MM gas-phase data when both ions are inside the stem. However, the results evidently resemble those from Figures 3 and 7, that is, moving one ion through two-quartet and three-quartet stems.

Symmetry-Adapted Perturbation Theory (SAPT). To further understand the differences between the QM and MM gas-phase calculations, we performed SAPT0 calculations using the jun-cc-pVDZ basis set for Na^+ and def2-SVPD basis set and corresponding auxiliary basis sets from the Turbomole library for K^+. We have calculated the path shown in Figure 8 with and without inclusion of the fixed ion. Two entities need to be defined for the SAPT0 interaction energy computations. We defined the moving cation as one entity and the two-quartet stem (plus the fixed cation in the two-ion case) as the other entity. Thus, interaction energies between the moving cation and the rest of the system are studied (Figure 14).

The SAPT0 method denotes the zeroth-order SAPT theory, which neglects intra-monomer correlation energy. The usually difficult to capture dispersion effects are small in our case (vide infra), so that errors stemming from any dispersion terms are

dx.doi.org/10.1021/ct4009969 | J. Chem. Theory Comput. 2014, 10, 1326−1340

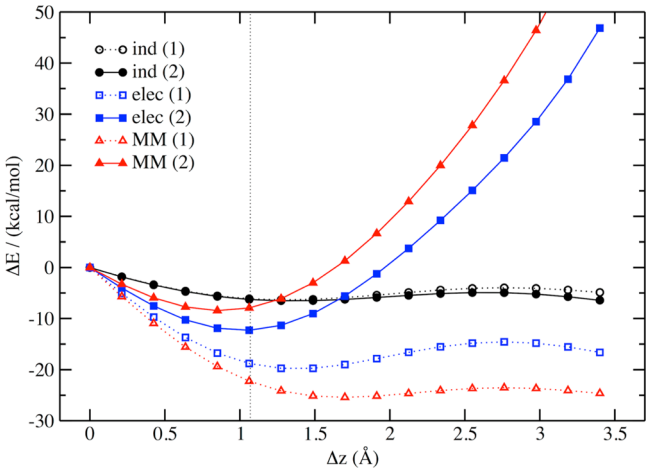

Figure 14. SAPT0 interaction energy component changes (kcal/mol) for the two-ion (2) and one-ion (1) model systems with two quartets and Na^+. The interaction energy decomposition is shown only for induction (ind) and electrostatics (elec). Molecular mechanical force field electrostatics is denoted as MM. The calculations follow the same path as shown in Figure 8; the two-ion and one-ion system includes and excludes the fixed ion, respectively. The interaction energy is defined between the moving ion and the rest of the system. The vertical line marks passage of the ion through the quartet plane.

also small. Of primary interest is the change in the interaction energy components along the scan and the difference between the one-ion and two-ion scans. The total interaction energy is reported in Table S13 of the Supporting Information.

Figure 14 shows the SAPT0 data for the induction/polarization (ind) and electrostatics (elec) terms for the one-ion (1) and two-ion (2) system with Na^+. The figure also includes the Coulomb term of the AMBER force field (MM). The induction term is similar for both studied systems. However, there is a significant change in the electrostatics, including a major difference between the QM and MM descriptions. The MM electrostatics curve for the two-ion system is more repulsive than the SAPT0 curve, while for the one-ion system it is more attractive. Furthermore, the MM minimum for the one-ion system is displaced by ~0.3 Å closer to the center of the quadruplex model compared to the SAPT0 results. The exchange interaction term (Figure S9, Supporting Information) is similar in both studied systems and is omitted from Figure 14 together with the very small dispersion term (essentially zero).

The reversal of the difference between the QM and MM electrostatics terms when investigating the one-ion and two-ion cases reflects the QM vs MM difference between the one-ion and two-ion scans discussed earlier in this study. At first sight, it may be confusing that we now capture this difference using the electrostatic term. This can be explained by the partitioning of the system used in the SAPT calculations. The densities of the monomer fragments are relaxed before the calculation of the inter-molecular electrostatics, that is, polarization of the two-quartet stem by the fixed ion occurs already on the fragment level and before the inter-molecular SAPT terms are calculated. This alters the formal SAPT electrostatic interactions between the moving ion and the quadruplex-ion fragment compared to the one-ion case. This explains why the above-discussed polarization effects missing in the force field description formally appear in the electrostatic term in SAPT computations.

The MM electrostatic curve for the two-ion system rises more steeply than the SAPT curve, which can be explained by the fact that the fixed +1 point charges of the MM cations cause a significant inter-cation repulsion, which is reduced in SAPT by the relaxation of the fragment density of the "fixed ion two-quartet stem" subsystem as described above.

The overestimation of the MM electrostatics attraction for the one-ion case could be partially attributed to the approximation of the force field as the fixed point charges do not account for induction/polarization effects.[67] The MM electrostatics would be indeed closer to the sum of SAPT induction and electrostatics for the one-ion case. This could explain the rather reasonable agreement between QM and MM for the one-ion curves shown in the previous sections. However, it also cannot be ruled out that the difference between QM and MM electrostatics for the one-ion case is due to simplicity of the point charge MM model. We did not investigate this issue in more detail.

The small changes in the induction term between the one-ion and two-ion case show that the presence of the fixed ion does not affect the subsequent polarization effects arising from the mobile ion, suggesting that both ions in the system cause an almost equal amount of polarization to the G-stem.

Figure S10 of the Supporting Information shows analogous computations for K^+, which confirm the SAPT data for Na^+.

QTAIM Analysis. To further probe the polarization of the electron density that accompanies movement of the ion, we have performed QTAIM analysis for two-quartet stem interacting with one or two Na^+ cations. We have taken three points from the scan shown in Figure 8. The upper (fixed) ion was omitted in the single-ion scan. The "out" position corresponds to the starting point in Figure 8, with the moving ion 1.0625 Å away from the proximal quartet. The "plane" position corresponds to ion position in the plane of the bottom quartet. The "in" position corresponds to the cavity center. We analyzed atomic charges and dipoles (also known as intra-atomic polarization) for symmetry-unique atoms. In this paragraph, the term "dipole" is used within the context of the QTAIM theory and implies that electron density is not uniformly (i.e., spherically) distributed around the atomic basin due to the proximity of neighboring atoms, which gives rise to the "intra-atomic dipole" according to the QTAIM terminology. A plethora of bond critical points (BCPs) corresponding to noncovalent interactions were located, including intra-quartet (Hoogsteen H-bonding), inter-quartet (π-stacking), and ion-base contacts (Figure S11, Supporting Information). These are not discussed in detail because they experience few changes as the ion moves along the scan path. However, in the "out" and "plane" geometries, four O6...Na^+ contacts exist with the bottom ion, whereas for the "in" geometry, eight such contacts are present. Also, the "in" form of the two-ion Na^+ system contains a BCP corresponding to a direct contact between ions (Figure S12, Supporting Information).

Individual atomic charge and dipole moments provide more insight and complement the SAPT0 data. In the single-ion case (Table S14, Supporting Information), each O6 in the "bottom" (Figure 8) quartet becomes more negative and less dipolar as the ion moves into its plane, and changes in the population and shape of N1 and H1 densities are also evident. However, changes in the "top" quartet are even larger as the ion moves into this geometry. This at first sight may look counterintuitive because the ion is located at the plane of the "bottom" quartet, and larger changes occur in the other quartet. The explanation

dx.doi.org/10.1021/ct4009969 | J. Chem. Theory Comput. 2014, 10, 1326−1340

is that the "bottom" quartet is already massively polarized by the ion in our reference (starting) "out" position, which is very close to it (Figure 8). Indeed, if the "out" position of the ion is selected to be at larger distance from the quartet (i.e., sufficiently far), then the largest changes would be observed on the "bottom" quartet. Moving the ion into the center of the system leads to much larger changes in the top quartet, which are largest for the H8, N3, C6, and O6 atoms. The latter atom in particular becomes markedly more negative and less dipolar in the proximity of the Na^+ compared to situation when the ion is outside the system. On the other hand, the bottom quartet O6 atoms become less negative, and dipoles modestly increase in magnitude when the ion is inserted to the center of the cavity, again compared to the starting "out" geometry. Other changes in the bottom quartet upon moving the ion into the center are generally small, although both H8 and H9 become slightly more positive with the ion inside the quartets. Also, it is noted that when the ion is at the center of the cavity the atomic data for the "bottom" and "top" quartets match due to symmetry.

The two-ions data (Table S15, Supporting Information) contrast with the single-ion case. Not only do the atomic charges change by much greater amounts (bearing in mind that at the reference "out" position the quartets are already polarized as noted above), but the trends along the path differ from the single-ion case. Moving Na^+ into the plane of the bottom quartet actually affects the top quartet slightly more, with both sets of O6 atoms becoming more negative and small changes elsewhere. Much larger changes are found on moving the ion into the center of the system, mainly in C6 and O6 but also in N3 atoms. The bottom N3 atom becomes less negative and less polarized, and the top N3 becomes also less negative and very slightly more polarized. Thus, QTAIM data shows that movement of the ion into the G-NA stem gives rise to substantial polarization, and moreove,r that the size and sign of such changes differ between the one-ion and two-ion cases.

Finally, for the single-ion case, the cation becomes markedly less positive and slightly less dipolar when shifted from the starting position to the quartet plane due to maximized polarization interaction with the quartet. When the second ion is present, the changes are similar but larger. When moving finally the ion to the center of the system without the second ion present, it becomes slightly more positive than at the initial position and substantially less dipolar. This is because in the final position it has less efficient contact with a quartet than in our specific starting position (Figure 8). This contrasts the two-ion case, where the moving ion becomes less positive and markedly more dipolar, exerting also a profound charge reduction effect on the fixed ion. In other words, there is a visible mutual reduction of the cation charges when the ions approach each other in the two-ion system compared to the equivalent positions in the one-ion system. The ion charges vary along the pathway in a complex manner. In summary, the QTAIM analysis highlights a complex pattern of polarization of the electron density as a function of ion position and number, and we postpone further analyses to a separate QTAIM study. Definitely, the data show that the system is not describable by any fixed charge model. Thus, although reduction of the cation charge within the framework of the fixed charge model could roughly reduce the excessive MM inter-cation repulsion, it would not be done in a physically correct way and would likely be accompanied by undesired side effects.

CONCLUDING REMARKS

Guanine quadruplex (G-DNA and G-RNA, i.e., G-NA) molecules represent an important class of noncanonical nucleic acids structures. Quadruplex molecules have been in the past investigated by computational techniques, mainly by explicit solvent molecular dynamics simulations with pair-additive force fields.[20−63,66] Because of an increase in computational power, quadruplex simulations recently reached the microsecond time scale,[53−56] which allows major expansion of the quadruplex simulation studies. However, longer simulations are also prone to be affected by force field approximations.[59−61]

Simulation studies of G-NA molecules carried out so far indicated very good performance of the force field. Nevertheless, some discrepancies between theory and experiment have been noticed, ranging from local imperfectness of the ion dynamics in the G-stem up to instability of some important ion binding sites observed in experimental studies.[60−62]

In this study, we have carried out set state-of-the art DFT-D3 QM computations of the ion binding to G-NA stems and compared them with the standard MM description. The present computations provide unique insights into the limitations of pairwise-additive MM treatment of nucleic acids, explain a number of observations reported in earlier explicit solvent simulation studies of G-NA molecules, and may also serve as benchmarks for testing or parametrization of polarizable biomolecular force fields.[108−113]

First, we performed a series of PES scans of binding of one-ion (Li^+, Na^+, and K^+) to two- and three-quartet stems (without the sugar−phosphate backbone) (Figures 2 and 6). When considering binding of a single ion to a two-quartet stem, we observed a modest gas-phase difference between QM and MM levels (Figures 3 and 5). The single-ion binding is more favored at the MM level. This has been explained by the fact that the stabilizing interaction between the ion and each guanine of the stem is additive at the MM level. In contrast, at the QM level, the additional stabilization by each guanine becomes less efficient upon completing the G-quartets (Figure S2, Supporting Information). This effect is reminiscent of the inter-ligand polarization repulsion that reduces the energy gain of the ligand binding when increasing the number of ligands in the cation coordination shell.[105−107] Nevertheless, employment of continuum solvent models (COSMO at QM and PBSA at MM level) basically eliminates the gas-phase differences between the QM and MM descriptions of binding of a single cation to the stem. Similar results were obtained also for binding of a single ion to a three-quartet stem (Figure 7). On the basis of the results, we suggest that the MM description of a binding of a single ion to G-NA stems is satisfactory and should not significantly bias explicit solvent MD simulations.

The above conclusion has to be sharply revisited when considering the biochemically more relevant binding of multiple ions to the G-stem (Figures 8 and 10). Binding of a second ion to a two-quartet stem is accompanied by large overestimation of the inter-cation repulsion at the MM level of description. This leads, for all three cation types considered, to sizable QM vs MM gas-phase energy differences of the order of 20 kcal/mol (Figure 9). The discrepancy is due to a lack of polarization term at the MM description. Polarization effects between the G-stem and the bound ion reduce the energy cost of binding a second ion by indirectly reducing the electrostatic repulsion of the cations. We suggest that the discrepancy cannot be corrected with the presently used MM formalism

utilizing constant atomic charges. Importantly, the continuum solvation models do not eliminate this discrepancy. Also, PES scans done for the three-quartet stem confirm the large overestimation of the cation−cation repulsion by MM (Figure 11).

For the sake of completeness, we have also carried out calculations with the GBSA MM approach. We found that calculations done with the GBSA MM method, at least with its presently used variant, differ substantially from the COSMO and MM-PBSA data. Although full analysis of this problem is beyond the scope of the paper, we suggest that the GBSA method is not reliable enough for studies of ion binding to quadruplexes.

The above findings are verified by symmetry-adapted perturbation theory calculations. Changes in the induction and electrostatic terms of the SAPT0 energy decomposition provide insights in the degree of polarization that occurs in the systems due to the cation−G-stem interactions. The PES scans (Figure 14) show that the lack of induction (polarization) in the MM description leads to the incorrect description of the electrostatics of the system by the force field in case of binding of multiple ions to the G-stem.

Further verification of the results was obtained by QTAIM analysis of the QM wave functions. These calculations support the view that binding of cations induces substantial polarization of guanines, with O6 atomic charges and atomic dipole moments (also referred to as intra-atomic polarization) being particularly strongly affected. Also the cation atomic charges are substantially affected, confirming limitations of methods utilizing constant atomic charges to describe binding of cations to the G-DNA stems. Importantly, the size and even sign of these changes are quite different depending on whether one or two ions are present. These effects will be difficult to properly describe using a nonpolarizable force field.

The polarization effects studied in our work may be also relevant to ion channel studies.[114−116] However, for the ion channels, the limitations of the pair-additive MM can be more complicated and of different balance between various many body effects because the ion transport typically involves cation−water−cation chains, and solute−solvent polarization effects are also present.[117] In quadruplexes, we deal with a chain of closely spaced, directly interacting cations, and thus the effect of polarization on the inter-cation interaction is predicted to be dramatic. Therefore, limitations in the description of ion transport systems are similar in origin but with further complications to the findings of this study, so that they cannot be straightforwardly extrapolated from this work. Note also that such water−ion chains in G-quadruplex channels have also been studied.[118]

On the basis of the results, we suggest that the cation dynamics seen in contemporary explicit solvent quadruplex MD simulations is inevitably biased by the MM approximation. We expect that the force field approximation likely distorts the correlation of the motions among the bound ions inside the stem, slows down binding of multiple ions to the G-stems, leads to excessively frequent expulsions of cations from the stems, and finally, destabilizes ion binding at the stem−loop junctions. The discrepancy will affect studies analyzing the structural dynamics as well as studies calculating free energies of the bound ions. Our work explains several problems reported in earlier explicit solvent simulation studies of quadruplex nucleic acid.[60−62]

■ ASSOCIATED CONTENT

Supporting Information

Schematic representation of the helical twist between opposite orientation quartets. Detailed data of reported PES curves: PES curves of K^+ with 1 up to 4 guanines kept in the geometries of the quartet, PES curves of 1ion/2quartet system with K^+ with respect to cation position at the cavity center, schematic representation of the opening of a quartet, PES curves for the one-ion/two-quartet system with K^+, Na^+, and Li^+ ions using the B3LYP cavity size corresponding to Na^+, PES curves for K^+, Na^+, Li^+ penetrating an expanded quartet, PES curves for the two-ion/two-quartet system with K^+, Na^+, and Li^+ ions using the B3LYP cavity size corresponding to Na^+, PES curve of two approaching K^+ ions, SAPT interaction energies for two-quartet/1 and 2 Na^+ systems, plot of SAPT exchange energy interaction component of Figure 14, SAPT curves for two-quartet/1 and 2 K^+ systems, QTAIM molecular graphs and data of atomic properties, and Cartesian coordinates of selected key geometries. This material is available free of charge via the Internet at http://pubs.acs.org.

■ AUTHOR INFORMATION

Corresponding Author

*E-mail: sponer@ncbr.muni.cz.

Notes

The authors declare no competing financial interest.

■ ACKNOWLEDGMENTS

This work was supported by the Czech Science Foundation (Grant P208/11/1822), project "CEITEC − Central European Institute of Technology" (CZ.1.05/1.1.00/02.0068) from European Regional Development Fund, and EU Seventh Framework Programme under the "Capacities" specific programme (Contract 286154).

■ REFERENCES

(1) Burge, S.; Parkinson, G. N.; Hazel, P.; Todd, A. K.; Neidle, S. Quadruplex DNA: Sequence, topology and structure. *Nucleic Acids Res.* **2006**, *34*, 5402−5415.

(2) Neidle, S. The structures of quadruplex nucleic acids and their drug complexes. *Curr. Opin. Struct. Biol.* **2009**, *19*, 239−250.

(3) Li, J.; Correia, J. J.; Wang, L.; Trent, J. O.; Chaires, J. B. Not so crystal clear: The structure of the human telomere G-quadruplex in solution differs from that present in a crystal. *Nucleic Acids Res.* **2005**, *33*, 4649−4659.

(4) Lane, A. N.; Chaires, J. B.; Gray, R. D.; Trent, J. O. Stability and kinetics of G-quadruplex structures. *Nucleic Acids Res.* **2008**, *36*, 5482−5515.

(5) Adrian, M.; Heddi, B.; Phan, A. T. NMR spectroscopy of G-quadruplexes. *Methods* **2012**, *57*, 11−24.

(6) Huppert, J. Quadruplexes in the Genome. In *Quadruplex Nucleic Acids*, 1stt ed.; Neidle, S., Balasubramanian, S., Eds.; RSC Biomolecular Sciences; The Royal Society of Chemistry:: Cambridge, U.K., 2006; pp 208−227.

(7) Da Silva, M. W.; Karsisiotis, A. I. Fundamentals and Applications of the Geometric Formalism of Quadruplex Folding. In *Guanine Quartets: Structure and Application*, 1st ed.; Fritzsche, W., Spindler, L., Eds.; The Royal Society of Chemistry:: Cambridge, U.K., 2013; pp 167−178.

(8) Mukundan, V. T.; Phan, A. T. Bulges in G-quadruplexes: Broadening the definition of G-quadruplex-forming sequences. *J. Am. Chem. Soc.* **2013**, *135*, 5017−5028.

(9) Šket, P.; Virgilio, A.; Esposito, V.; Galeone, A.; Plavec, J. Strand directionality affects cation binding and movement within tetramolecular G-quadruplexes. *Nucleic Acids Res.* **2012**, *40*, 11047−11057.

(10) Trajkovski, M.; Plavec, J. Assessing roles of cations in G-quadruplex-based nanowires by NMR. *J. Phys. Chem. C* **2012**, *116*, 23821−23825.
(11) Maizels, N. Biological Functions of G-Quadruplexes. In *Guanine Quartets: Structure and Application*, 1st ed.; Fritzsche, W., Spindler, L., Eds.; The Royal Society of Chemistry: Cambridge, U.K., 2013; pp 215−222.
(12) Mergny, J.-L.; Mailliet, P.; Lavelle, F.; Riou, J.-F.; Laoui, A.; Hélène, C. The development of telomerase inhibitors: The G-quartet approach. *Anti-Cancer Drug Des.* **1999**, *14*, 327−339.
(13) Beaudoin, J.-D.; Perreault, J.-P. 5′-UTR G-quadruplex structures acting as translational repressors. *Nucleic Acids Res.* **2010**, *38*, 7022−7036.
(14) Bugaut, A.; Balasubramanian, S. 5′-UTR RNA G-quadruplexes: Translation regulation and targeting. *Nucleic Acids Res.* **2012**, *40*, 4727−4741.
(15) Gomez, D.; Guédin, A.; Mergny, J.-L.; Salles, B.; Riou, J.-F.; Teulade-Fichou, M.-P.; Calsou, P. A G-quadruplex structure within the 5′-UTR of TRF2 mRNA represses translation in human cells. *Nucleic Acids Res.* **2010**, *38*, 7187−7198.
(16) Huppert, J. L.; Bugaut, A.; Kumari, S.; Balasubramanian, S. G-quadruplexes: The beginning and end of UTRs. *Nucleic Acids Res.* **2008**, *36*, 6260−6268.
(17) Yatsunyk, L. A.; Piétrement, O.; Albrecht, D.; Tran, P. L. T.; Renčiuk, D.; Sugiyama, H.; Arbona, J.-M.; Aimé, J.-P.; Mergny, J.-L. Guided assembly of tetramolecular G-quadruplexes. *ACS Nano* **2013**, *7*, 5701−5710.
(18) Russo Krauss, I.; Pica, A.; Merlino, A.; Mazzarella, L.; Sica, F. Duplex-quadruplex motifs in a peculiar structural organization cooperatively contribute to thrombin binding of a DNA aptamer. *Acta Crystallogr., Sect. D: Biol. Crystallogr.* **2013**, *69*, 2403−2411.
(19) Yoshida, W.; Saito, T.; Yokoyama, T.; Ferri, S.; Ikebukuro, K. Aptamer selection based on G4-forming promoter region. *PLoS One* **2013**, *8*, e65497.
(20) Akhshi, P.; Mosey, N. J.; Wu, G. Free-energy landscapes of ion movement through a G-quadruplex DNA channel. *Angew. Chem., Int. Ed. Engl.* **2012**, *51*, 2850−2854.
(21) Lech, C. J.; Heddi, B.; Phan, A. T. Guanine base stacking in G-quadruplex nucleic acids. *Nucleic Acids Res.* **2013**, *41*, 2034−2046.
(22) Hou, J.-Q.; Chen, S.-B.; Tan, J.-H.; Luo, H.-B.; Li, D.; Gu, L.-Q.; Huang, Z.-S. New insights from molecular dynamic simulation studies of the multiple binding modes of a ligand with G-quadruplex DNA. *J. Comput.-Aided Mol. Des.* **2012**, *26*, 1355−1368.
(23) Krepl, M.; Zgarbová, M.; Stadlbauer, P.; Otyepka, M.; Banáš, P.; Koča, J.; Cheatham, T. E.; Jurečka, P.; Šponer, J. Reference simulations of noncanonical nucleic acids with different χ variants of the AMBER force field: Quadruplex DNA, quadruplex RNA, and Z-DNA. *J. Chem. Theory Comput.* **2012**, *8*, 2506−2520.
(24) Collie, G. W.; Haider, S. M.; Neidle, S.; Parkinson, G. N. A crystallographic and modelling study of a human telomeric RNA (TERRA) quadruplex. *Nucleic Acids Res.* **2010**, *38*, 5569−5580.
(25) Li, M.-H.; Zhou, Y.-H.; Luo, Q.; Li, Z.-S. The 3D structures of G-quadruplexes of HIV-1 integrase inhibitors: Molecular dynamics simulations in aqueous solution and in the gas phase. *J. Mol. Model.* **2010**, *16*, 645−657.
(26) Haider, S.; Neidle, S. Molecular Modeling and Simulation of G-Quadruplexes and Quadruplex-Ligand Complexes. In *G-Quadruplex DNA*, 1st ed.; Baumann, P., Ed.; Methods in Molecular Biology; Humana Press: New York, 2010; pp 17−37.
(27) Haider, S.; Parkinson, G. N.; Neidle, S. Molecular dynamics and principal components analysis of human telomeric quadruplex multimers. *Biophys. J.* **2008**, *95*, 296−311.
(28) Li, M.-H.; Luo, Q.; Xue, X.-G.; Li, Z.-S. Molecular dynamics studies of the 3D structure and planar ligand binding of a quadruplex dimer. *J. Mol. Model.* **2011**, *17*, 515−526.
(29) Hou, J.-Q.; Chen, S.-B.; Tan, J.-H.; Ou, T.-M.; Luo, H.-B.; Li, D.; Xu, J.; Gu, L.-Q.; Huang, Z.-S. New insights into the structures of ligand−quadruplex complexes from molecular dynamics simulations. *J. Phys. Chem. B* **2010**, *114*, 15301−15310.
(30) Woiczikowski, P. B.; Kubař, T.; Gutiérrez, R.; Cuniberti, G.; Elstner, M. Structural stability versus conformational sampling in biomolecular systems: Why is the charge transfer efficiency in G4-DNA better than in double-stranded DNA? *J. Chem. Phys.* **2010**, *133*, 035103.
(31) Li, M.-H.; Luo, Q.; Li, Z.-S. Molecular dynamics study on the interactions of porphyrin with two antiparallel human telomeric quadruplexes. *J. Phys. Chem. B* **2010**, *114*, 6216−6224.
(32) Cavallari, M.; Garbesi, A.; Di Felice, R. Porphyrin intercalation in G4-DNA quadruplexes by molecular dynamics simulations. *J. Phys. Chem. B* **2009**, *113*, 13152−13160.
(33) Li, H.; Cao, E.; Gisler, T. Force-induced unfolding of human telomeric G-quadruplex: A steered molecular dynamics simulation study. *Biochem. Biophys. Res. Commun.* **2009**, *379*, 70−75.
(34) Arora, A.; Balasubramanian, C.; Kumar, N.; Agrawal, S.; Ojha, R. P.; Maiti, S. Binding of berberine to human telomeric quadruplex − Spectroscopic, calorimetric and molecular modeling studies. *FEBS J.* **2008**, *275*, 3971−3983.
(35) Cavallari, M.; Calzolari, A.; Garbesi, A.; Di Felice, R. Stability and migration of metal ions in G4-wires by molecular dynamics simulations. *J. Phys. Chem. B* **2006**, *110*, 26337−26348.
(36) Rueda, M.; Luque, F. J.; Orozco, M. G-quadruplexes can maintain their structure in the gas phase. *J. Am. Chem. Soc.* **2006**, *128*, 3608−3619.
(37) Moore, M. J. B.; Schultes, C. M.; Cuesta, J.; Cuenca, F.; Gunaratnam, M.; Tanious, F. A.; Wilson, W. D.; Neidle, S. Trisubstituted acridines as G-quadruplex telomere targeting agents. Effects of extensions of the 3,6- and 9-side chains on quadruplex binding, telomerase activity, and cell proliferation. *J. Med. Chem.* **2006**, *49*, 582−599.
(38) Hazel, P.; Parkinson, G. N.; Neidle, S. Predictive modelling of topology and loop variations in dimeric DNA quadruplex structures. *Nucleic Acids Res.* **2006**, *34*, 2117−2127.
(39) Hazel, P.; Huppert, J.; Balasubramanian, S.; Neidle, S. Loop-length-dependent folding of G-quadruplexes. *J. Am. Chem. Soc.* **2004**, *126*, 16405−16415.
(40) Petraccone, L.; Erra, E.; Esposito, V.; Randazzo, A.; Mayol, L.; Nasti, L.; Barone, G.; Giancola, C. Stability and structure of telomeric DNA sequences forming quadruplexes containing four G-tetrads with different topological arrangements. *Biochemistry* **2004**, *43*, 4877−4884.
(41) Štefl, R.; Špačková, N.; Berger, I.; Koča, J.; Šponer, J. Molecular dynamics of DNA quadruplex molecules containing inosine, 6-thioguanine and 6-thiopurine. *Biophys. J.* **2001**, *80*, 455−468.
(42) Chaubey, A. K.; Dubey, K. D.; Ojha, R. P. Stability and free energy calculation of LNA modified quadruplex: A molecular dynamics study. *J. Comput.-Aided Mol. Des.* **2012**, *26*, 289−299.
(43) Andrushchenko, V.; Tsankov, D.; Krasteva, M.; Wieser, H.; Bour, P. Spectroscopic detection of DNA quadruplexes by vibrational circular dichroism. *J. Am. Chem. Soc.* **2011**, *133*, 15055−15064.
(44) Han, H.; Langley, D. R.; Rangan, A.; Hurley, L. H. Selective interactions of cationic porphyrins with G-quadruplex structures. *J. Am. Chem. Soc.* **2001**, *123*, 8902−8913.
(45) Read, M. A.; Neidle, S. Structural characterization of a guanine−quadruplex ligand complex. *Biochemistry* **2000**, *39*, 13422−13432.
(46) Šponer, J.; Špačková, N. Molecular dynamics simulations and their application to four-stranded DNA. *Methods* **2007**, *43*, 278−290.
(47) Akhshi, P.; Acton, G.; Wu, G. Molecular dynamics simulations to provide new insights into the asymmetrical ammonium ion movement inside of the $[d(G_3T_4G_4)]_2$ G-quadruplex DNA structure. *J. Phys. Chem. B* **2012**, *116*, 9363−9370.
(48) Novotný, J.; Kulhánek, P.; Marek, R. Biocompatible xanthine-quadruplex scaffold for ion-transporting DNA channels. *J. Phys. Chem. Lett.* **2012**, *3*, 1788−1792.
(49) Chowdhury, S.; Bansal, M. G-quadruplex structure can be stable with only some coordination sites being occupied by cations: A six-nanosecond molecular dynamics study. *J. Phys. Chem. B* **2001**, *105*, 7572−7578.
(50) Štefl, R.; Cheatham, T. E.; Špačková, N.; Fadrná, E.; Berger, I.; Koča, J.; Šponer, J. Formation pathways of a guanine-quadruplex DNA

revealed by molecular dynamics and thermodynamic analysis of the substates. *Biophys. J.* **2003**, *85*, 1787−1804.
(51) Špačková, N.; Berger, I.; Šponer, J. Structural dynamics and cation interactions of DNA quadruplex molecules containing mixed guanine/cytosine quartets revealed by large-scale MD simulations. *J. Am. Chem. Soc.* **2001**, *123*, 3295−3307.
(52) Pagano, B.; Mattia, C. A.; Cavallo, L.; Uesugi, S.; Giancola, C.; Fraternali, F. Stability and cations coordination of DNA and RNA 14-Mer G-quadruplexes: A multiscale computational approach. *J. Phys. Chem. B* **2008**, *112*, 12115−12123.
(53) Reshetnikov, R.; Golovin, A.; Spiridonova, V.; Kopylov, A.; Šponer, J. Structural dynamics of thrombin-binding DNA aptamer d(GGTTGGTGTGGTTGG) quadruplex DNA studied by large-scale explicit solvent simulations. *J. Chem. Theory Comput.* **2010**, *6*, 3003−3014.
(54) Reshetnikov, R. V.; Šponer, J.; Rassokhina, O. I.; Kopylov, A. M.; Tsvetkov, P. O.; Makarov, A. A.; Golovin, A. V. Cation binding to 15-TBA quadruplex DNA is a multiple-pathway cation-dependent process. *Nucleic Acids Res.* **2011**, *39*, 9789−9802.
(55) Zhu, H.; Xiao, S.; Liang, H. Structural dynamics of human telomeric G-quadruplex loops studied by molecular dynamics simulations. *PLoS One* **2013**, *8*, e71380.
(56) Islam, B.; Sgobba, M.; Laughton, C.; Orozco, M.; Šponer, J.; Neidle, S.; Haider, S. Conformational dynamics of the human propeller telomeric DNA quadruplex on a microsecond time scale. *Nucleic Acids Res.* **2013**, *41*, 2723−2735.
(57) Stadlbauer, P.; Krepl, M.; Cheatham, T. E.; Koča, J.; Šponer, J. Structural dynamics of possible late-stage intermediates in folding of quadruplex DNA studied by molecular simulations. *Nucleic Acids Res.* **2013**, *41*, 7128−7143.
(58) Limongelli, V.; De Tito, S.; Cerofolini, L.; Fragai, M.; Pagano, B.; Trotta, R.; Cosconati, S.; Marinelli, L.; Novellino, E.; Bertini, I.; Randazzo, A.; Luchinat, C.; Parrinello, M. The G-triplex DNA. *Angew. Chem.* **2013**, *125*, 2325−2329.
(59) Šponer, J.; Cang, X.; Cheatham, T. E. Molecular dynamics simulations of G-DNA and perspectives on the simulation of nucleic acid structures. *Methods* **2012**, *57*, 25−39.
(60) Špačková, N.; Berger, I.; Šponer, J. Nanosecond molecular dynamics simulations of parallel and antiparallel guanine quadruplex DNA molecules. *J. Am. Chem. Soc.* **1999**, *121*, 5519−5534.
(61) Fadrná, E.; Špačková, N.; Štefl, R.; Koča, J.; Cheatham, T. E.; Šponer, J. Molecular dynamics simulations of guanine quadruplex loops: Advances and force field limitations. *Biophys. J.* **2004**, *87*, 227−242.
(62) Fadrná, E.; Špačková, N.; Sarzyñska, J.; Koča, J.; Orozco, M.; Cheatham, T. E.; Kulinski, T.; Šponer, J. Single stranded loops of quadruplex DNA as key benchmark for testing nucleic acids force fields. *J. Chem. Theory Comput.* **2009**, *5*, 2514−2530.
(63) Cang, X.; Šponer, J.; Cheatham, T. E. Explaining the varied glycosidic conformational, G-tract length and sequence preferences for anti-parallel G-quadruplexes. *Nucleic Acids Res.* **2011**, *39*, 4499−4512.
(64) Šponer, J.; Mládek, A.; Špačková, N.; Cang, X.; Cheatham, T. E.; Grimme, S. Relative stability of different DNA guanine quadruplex stem topologies derived using large-scale quantum-chemical computations. *J. Am. Chem. Soc.* **2013**, *135*, 9785−9796.
(65) Šponer, J.; Mládek, A.; Šponer, J. E.; Svozil, D.; Zgarbová, M.; Banáš, P.; Jurečka, P.; Otyepka, M. The DNA and RNA sugar-phosphate backbone emerges as the key player. An overview of quantum-chemical, structural biology and simulation studies. *Phys. Chem. Chem. Phys.* **2012**, *14*, 15257−15277.
(66) Song, J.; Ji, C.; Zhang, J. Z. H. The critical effect of polarization on the dynamical structure of guanine quadruplex DNA. *Phys. Chem. Chem. Phys.* **2012**, *15*, 3846−3854.
(67) Cornell, W. D.; Cieplak, P.; Bayly, C. I.; Gould, I. R.; Merz, K. M.; Ferguson, D. M.; Spellmeyer, D. C.; Fox, T.; Caldwell, J. W.; Kollman, P. A. A second generation force field for the simulation of proteins, nucleic acids, and organic molecules. *J. Am. Chem. Soc.* **1995**, *117*, 5179−5197.
(68) Fonseca Guerra, C.; van der Wijst, T.; Poater, J.; Swart, M.; Bickelhaupt, F. M. Adenine versus guanine quartets in aqueous solution: Dispersion-corrected DFT study on the differences in p-stacking and hydrogen-bonding behavior. *Theor. Chem. Acc.* **2010**, *125*, 245−252.
(69) Meyer, M.; Hocquet, A.; Sühnel, J. Interaction of sodium and potassium ions with sandwiched cytosine-, guanine-, thymine-, and uracil-base tetrads. *J. Comput. Chem.* **2005**, *26*, 352−364.
(70) Otero, R.; Schöck, M.; Molina, L. M.; Lægsgaard, E.; Stensgaard, I.; Hammer, B.; Besenbacher, F. Guanine quartet networks stabilized by cooperative hydrogen bonds. *Angew. Chem., Int. Ed.* **2005**, *44*, 2270−2275.
(71) Gu, J.; Leszczynski, J. Origin of Na^+/K^+ selectivity of the guanine tetraplexes in water: The theoretical rationale. *J. Phys. Chem. A* **2002**, *106*, 529−532.
(72) Louit, G.; Hocquet, A.; Ghomi, M.; Meyer, M.; Sühnel, J. Are guanine tetrads stabilised by bifurcated hydrogen bonds? An AIM topological analysis of the electronic density. *PhysChemComm* **2002**, *5*, 94−98.
(73) Meyer, M.; Steinke, T.; Brandl, M.; Sühnel, J. Density functional study of guanine and uracil quartets and of guanine quartet/metal ion complexes. *J. Comput. Chem.* **2001**, *22*, 109−124.
(74) van Mourik, T.; Dingley, A. J. Characterization of the monovalent ion position and hydrogen-bond network in guanine quartets by DFT calculations of NMR parameters. *Chem.—Eur. J.* **2005**, *11*, 6064−6079.
(75) Gu, J.; Leszczynski, J. A remarkable alteration in the bonding pattern: An HF and DFT study of the interactions between the metal cations and the Hoogsteen hydrogen-bonded G-tetrad. *J. Phys. Chem. A* **2000**, *104*, 6308−6313.
(76) Louit, G.; Hocquet, A.; Ghomi, M.; Meyer, M.; Sühnel, J. Guanine tetrads interacting with metal ions. An AIM topological analysis of the electronic density. *PhysChemComm* **2003**, *6*, 1−5.
(77) Gresh, N.; Pullman, B. A theoretical study of the selective entrapment of alkali and ammonium cations between guanine tetramers. *Int. J. Quantum Chem., Quantum Biol. Symp.* **1986**, *28*, 49−56.
(78) Staroverov, V. N.; Scuseria, G. E.; Tao, J.; Perdew, J. P. Comparative assessment of a new nonempirical density functional: Molecules and hydrogen-bonded complexes. *J. Chem. Phys.* **2003**, *119*, 12129.
(79) Grimme, S.; Ehrlich, S.; Goerigk, L. Effect of the damping function in dispersion corrected density functional theory. *J. Comput. Chem.* **2011**, *32*, 1456−1465.
(80) Grimme, S.; Antony, J.; Ehrlich, S.; Krieg, H. A consistent and accurate ab initio parametrization of density functional dispersion correction (DFT-D) for the 94 elements H-Pu. *J. Chem. Phys.* **2010**, *132*, 154104.
(81) Schäfer, A.; Horn, H.; Ahlrichs, R. Fully optimized contracted Gaussian basis sets for atoms Li to Kr. *J. Chem. Phys.* **1992**, *97*, 2571−2577.
(82) Weigend, F.; Ahlrichs, R. Balanced basis sets of split valence, triple zeta valence and quadruple zeta valence quality for H to Rn: Design and assessment of accuracy. *Phys. Chem. Chem. Phys.* **2005**, *7*, 3297−3305.
(83) Eichkorn, K.; Treutler, O.; Öhm, H.; Häser, M.; Ahlrichs, R. Auxiliary basis sets to approximate Coulomb potentials. *Chem. Phys. Lett.* **1995**, *240*, 283−290.
(84) Weigend, F.; Köhn, A.; Hättig, C. Efficient use of the correlation consistent basis sets in resolution of the identity MP2 calculations. *J. Chem. Phys.* **2002**, *116*, 3175−3183.
(85) Neese, F. *ORCA-an Ab Initio, Density Functional and Semiempirical Program Package*, version 2.9.1; University of Bonn: Bonn, Germany, 2012.
(86) Frisch, M. J.; Trucks, G. W.; Schlegel, H. B.; Scuseria, G. E.; Robb, M. A.; Cheeseman, J. R.; Scalmani, G.; Barone, V.; Mennucci, B.; Petersson, G. A.; Nakatsuji, H.; Caricato, M.; Li, X.; Hratchian, H. P.; Izmaylov, A. F.; Bloino, J.; Zheng, G.; Sonnenberg, J. L.; Hada, M.; Ehara, M.; Toyota, K.; Fukuda, R.; Hasegawa, J.; Ishida, M.; Nakajima,

T.; Honda, Y.; Kitao, O.; Nakai, H.; Vreven, T.; Montgomery, J. A., Jr.; Peralta, J. E.; Ogliaro, F.; Bearpark, M.; Heyd, J. J.; Brothers, E.; Kudin, K. N.; Staroverov, V. N.; Kobayashi, R.; Normand, J.; Raghavachari, K.; Rendell, A.; Burant, J. C.; Iyengar, S. S.; Tomasi, J.; Cossi, M.; Rega, N.; Millam, N. J.; Klene, M.; Knox, J. E.; Cross, J. B.; Bakken, V.; Adamo, C.; Jaramillo, J.; Gomperts, R.; Stratmann, R. E.; Yazyev, O.; Austin, A. J.; Cammi, R.; Pomelli, C.; Ochterski, J. W.; Martin, R. L.; Morokuma, K.; Zakrzewski, V. G.; Voth, G. A.; Salvador, P.; Dannenberg, J. J.; Dapprich, S.; Daniels, A. D.; Farkas, Ö.; Foresman, J. B.; Ortiz, J. V.; Cioslowski, J.; Fox, D. J. Gaussian 09, revision D.01; Gaussian, Inc.: Wallingford, CT, 2009.

(87) Sinnecker, S.; Rajendran, A.; Klamt, A.; Diedenhofen, M.; Neese, F. Calculation of solvent shifts on electronic g-tensors with the conductor-like screening model (COSMO) and its self-consistent generalization to real solvents (direct COSMO-RS). *J. Phys. Chem. A* **2006**, *110*, 2235−2245.

(88) Klamt, A. The COSMO and COSMO-RS solvation models. *Wiley Interdiscip. Rev.: Comput. Mol. Sci.* **2011**, *1*, 699−709.

(89) Klamt, A.; Schüürmann, G. COSMO: A new approach to dielectric screening in solvents with explicit expressions for the screening energy and its gradient. *J. Chem. Soc., Perkin Trans. 2* **1993**, *2*, 799−805.

(90) Case, D. A.; Darden, T. A.; Cheatham, T. E., III; Simmerling, C. L.; Wang, J.; Duke, R. E.; Luo, R.; Walker, R. C.; Zhang, W.; Merz, K. M.; Roberts, B.; Hayik, S.; Roitberg, A.; Seabra, G.; Swails, J.; Goetz, A. W.; Kolossváry, I.; Wong, K. F.; Paesani, F.; Vanicek, J.; Wolf, R. M.; Liu, J.; Wu, X.; Brozell, S. R.; Steinbrecher, T.; Gohlke, H.; Cai, Q.; Ye, X.; Wang, J.; Hsieh, M.-J.; Cui, G.; Roe, D. R.; Mathews, D. H.; Seetin, M. G.; Salomon-Ferrer, R.; Sagui, C.; Babin, V.; Luchko, T.; Gusarov, S.; Kovalenko, A.; Kollman, P. A. *AMBER 12*, University of California: San Francisco, CA, 2012.

(91) Joung, I. S.; Cheatham, T. E., III Determination of alkali and halide monovalent ion parameters for use in explicitly solvated biomolecular simulations. *J. Phys. Chem. B* **2008**, *112*, 9020−9041.

(92) Hawkins, G. D.; Cramer, C. J.; Truhlar, D. G. Parametrized models of aqueous free energies of solvation based on pairwise descreening of solute atomic charges from a dielectric medium. *J. Phys. Chem.* **1996**, *100*, 19824−19839.

(93) Hawkins, G. D.; Cramer, C. J.; Truhlar, D. G. Pairwise solute descreening of solute charges from a dielectric medium. *Chem. Phys. Lett.* **1995**, *246*, 122−129.

(94) Tsui, V.; Case, D. A. Theory and applications of the generalized born solvation model in macromolecular simulations. *Biopolymers* **2000**, *56*, 275−291.

(95) Turney, J. M.; Simmonett, A. C.; Parrish, R. M.; Hohenstein, E. G.; Evangelista, F.; Fermann, J. T.; Mintz, B. J.; Burns, L. A.; Wilke, J. J.; Abrams, M. L.; Russ, N. J.; Leininger, M. L.; Janssen, C. L.; Seidl, E. T.; Allen, W. D.; Schaefer, H. F.; King, R. A.; Valeev, E. F.; Sherrill, C. D.; Crawford, T. D. Psi4: An open-source *ab initio* electronic structure program. *Wiley Interdiscip. Rev.: Comput. Mol. Sci.* **2012**, *2*, 556−565.

(96) Hohenstein, E. G.; Sherrill, C. D. Efficient evaluation of triple excitations in symmetry-adapted perturbation theory via second-order Møller−Plesset perturbation theory natural orbitals. *J. Chem. Phys.* **2010**, *133*, 104107.

(97) Hohenstein, E. G.; Sherrill, C. D. Density fitting and Cholesky decomposition approximations in symmetry-adapted perturbation theory: Implementation and application to probe the nature of $\pi-\pi$ interactions in linear acenes. *J. Chem. Phys.* **2010**, *132*, 184111.

(98) Hohenstein, E. G.; Parrish, R. M.; Sherrill, C. D.; Turney, J. M.; Schaefer, H. F. Large-scale symmetry-adapted perturbation theory computations via density fitting and Laplace transformation techniques: Investigating the fundamental forces of DNA-intercalator interactions. *J. Chem. Phys.* **2011**, *135*, 174107.

(99) Dunning, T. H., Jr. Gaussian basis sets for use in correlated molecular calculations. I. The atoms boron through neon and hydrogen. *J. Chem. Phys.* **1989**, *90*, 1007−1023.

(100) Kendall, R. A.; Dunning, T. H., Jr.; Harrison, R. J. Electron affinities of the first-row atoms revisited. Systematic basis sets and wave functions. *J. Chem. Phys.* **1992**, *96*, 6796−6806.

(101) Woon, D. E.; Dunning, T. H., Jr. Gaussian basis sets for use in correlated molecular calculations. III. The atoms aluminum through argon. *J. Chem. Phys.* **1993**, *98*, 1358−1371.

(102) Bader, R. F. W. *Atoms In Molecules − A Quantum Theory*; Oxford University Press: London, 1990.

(103) Keith, T. A. *AIMAll*, version 13.05.06; TK Gristmill Software: Overland Park, KS, 2013.

(104) de Courcy, B.; Piquemal, J.-P.; Gresh, N. Energy analysis of Zn polycoordination in a metalloprotein environment and of the role of a neighboring aromatic residue. What is the impact of polarization? *J. Chem. Theory Comput.* **2008**, *4*, 1659−1668.

(105) Šponer, J.; Burda, J. V.; Sabat, M.; Leszczynski, J.; Hobza, P. Interaction between the guanine−cytosine Watson−Crick DNA base pair and hydrated group IIa (Mg^{2+}, Ca^{2+}, Sr^{2+}, Ba^{2+}) and group IIb (Zn^{2+}, Cd^{2+}, Hg^{2+}) metal cations. *J. Phys. Chem. A* **1998**, *102*, 5951−5957.

(106) Hartmann, M.; Clark, T.; van Eldik, R. Hydration and water exchange of zinc(II) Ions. Application of density functional theory. *J. Am. Chem. Soc.* **1997**, *119*, 7843−7850.

(107) Bock, C. W.; Katz, A. K.; Glusker, J. P. Hydration of zinc ions: A comparison with magnesium and beryllium ions. *J. Am. Chem. Soc.* **1995**, *117*, 3754−3763.

(108) Gresh, N.; Garmer, D. R. Comparative binding energetics of Mg^{2+}, Ca^{2+}, Zn^{2+}, and Cd^{2+} to biologically relevant ligands: Combined ab initio SCF supermolecule and molecular mechanics investigation. *J. Comput. Chem.* **1996**, *17*, 1481−1495.

(109) Halgren, T. A.; Damm, W. Polarizable force fields. *Curr. Opin. Struct. Biol.* **2001**, *11*, 236−242.

(110) Gresh, N.; Šponer, J. E.; Špačková, N.; Leszczynski, J.; Šponer, J. Theoretical study of binding of hydrated Zn(II) and Mg(II) cations to 5′-guanosine monophosphate. Toward polarizable molecular mechanics for DNA and RNA. *J. Phys. Chem. B* **2003**, *107*, 8669−8681.

(111) Gresh, N.; Cisneros, G. A.; Darden, T. A.; Piquemal, J.-P. Anisotropic, polarizable molecular mechanics studies of inter- and intramolecular interactions and ligand-macromolecule complexes. A bottom-up strategy. *J. Chem. Theory Comput.* **2007**, *3*, 1960−1986.

(112) Cieplak, P.; Dupradeau, F.-Y.; Duan, Y.; Wang, J. Polarization effects in molecular mechanical force fields. *J. Phys.: Condens. Matter* **2009**, *21*, 333102.

(113) Shi, Y.; Xia, Z.; Zhang, J.; Best, R.; Wu, C.; Ponder, J. W.; Ren, P. Polarizable atomic multipole-based AMOEBA force field for proteins. *J. Chem. Theory Comput.* **2013**, *9*, 4046−4063.

(114) Illingworth, C. J. R.; Furini, S.; Domene, C. Computational studies on polarization effects and selectivity in K^+ channels. *J. Chem. Theory Comput.* **2010**, *6*, 3780−3792.

(115) Compoint, M.; Ramseyer, C.; Huetz, P. Ab initio investigation of the atomic charges in the KcsA channel selectivity filter. *Chem. Phys. Lett.* **2004**, *397*, 510−515.

(116) Sansom, M. S. P.; Shrivastava, I. H.; Bright, J. N.; Tate, J.; Capener, C. E.; Biggin, P. C. Potassium channels: Structures, models, simulations. *Biochim. Biophys. Acta* **2002**, *1565*, 294−307.

(117) Choi, C. H.; Re, S.; Rashid, M. H. O.; Li, H.; Feig, M.; Sugita, Y. Solvent electronic polarization effects on Na^+−Na^+ and Cl^-−Cl^- pair associations in aqueous solution. *J. Phys. Chem. B* **2013**, *117*, 9273−9279.

(118) Ngo, V. A.; Di Felice, R.; Haas, S. Is the G-quadruplex an effective nanoconductor for ions? *J. Phys. Chem. B* **2014**, *118*, 864−872.